Journal of Ovonic Research Vol. 17, No. 1, January - February 2021, p. 11 - 21

THEORETICAL SIMULATION OF THE EFFECT OF TEMPERATURE OF MULTI-JUNCTION SOLAR CELLS (PIN/ InGaN)

L. MOUSLI[a,*], B. DENNAI[b], B. AZEDDINE[c]
[a]*Laboratory Smart Grid and Renewable Energy, University Tahri Mohammed Béchar, Algeria*
[b]*Laboratory of Renewable Energy development and their applications in the Saharan areas University Tahri Mohammed, Béchar, Algeria*
[c]*Laboratory of Physics and Semiconductors devises, University Tahri Mohammed, Béchar, Algeria*

In this study, we performed a numerical theoretical simulation of single-junction and dual-junction solar cells based on InGaN. This simulation calculates the electrical parameters, characteristics of each of the studied cells, such as absorption, open-circuit voltage (V_{co}), collection efficiency, short circuit density (J_{sc}), and form factor FF. We have optimized the cells top PIN ($In_{0.62}Ga_{0.38}N$) and bottom PIN ($In_{0.81}Ga_{0.19}N$), and a dual-junction cell. The conversation efficiency of the single junction PIN cells exceeds 23%, while it is 38% for the dual-junction cell. The temperature dependencies of single junction and dual-junction solar cells have been studied at temperatures ranging from 300˚K to 450˚K. The variation of the electrical parameters of each cell was simulated with increasing temperature and the simulation result was detailed in this study. This study was done under standard conditions (AM1.5, 1000mW/cm^2) and the simulation was performed on an ANOC calculation code (the latter is available as an application on android devices).

(Received September 27, 2020 ; Accepted January 9, 2021)

Keywords: InGaN, PIN, Temperature, Tandem, Efficiency, Molar fraction, ANOC

1. Introduction

The material used in this work is the gallium indium nitride this material is a semiconductor in the category of nitride III, which represents a new category of materials with important properties for optoelectronics, such as light-emitting diodes and solar cells [1]. The application of these alloys is predetermined by the very interesting absorption coefficient and the high conversion efficiency (may exceed 40%) with super radiation resistance. The advantage of this "InGaN" alloy is its forbidden band (gap) [2], possess the characteristic of a direct gap, which allows it to absorb a fairly large part of the solar spectrum, such as the InN established with a prohibited energy band of 0.7 eV [3]. For GaN, the prohibited band is 3.42 eV [3]. In this work, in the first place, an analytical study is proposed, to study the performance of tandem solar cells based on InGaN (PIN). We evaluate the characteristics of the cell to define the optimal structure of the device. In the second phase of this study, we are interested in the influence of temperature on cell characteristics on the one hand, and on the other hand, we have studied the effect of gaps energy is their influence on the electrical efficiency of the structure, in the case of a single junction and tandem.

2. Theoretical modeling

Multi-junction PIN (tandem) solar cells represent some advantages over single PIN cells or PN cells. The integration of an intrinsic layer to improve the absorption of the solar spectrum, which is considered an important factor for the design of a photovoltaic cell based on a PIN structure.

[*] Corresponding author: latifalolo1977@gmail.com

Fig. 1 shows the structure of an InGaN-based multi-junction solar cell for simulation. The thickness of the active P layer is assumed to be 250nm for the top cell, the thickness of the intrinsic layer is optimized; so that the field remains important to separate the electron-holes generated in this area. The characteristic parameters of the solar cells were simulated based on the molar fraction, and the temperature. The numerical simulation of the InGaN-based multi-junction solar cell was performed using an ' ANOC ' calculation code, under standard conditions (1 sun, AM1.5, 300˚K to 450˚K). In this study, it was assumed that for the calculation of electrical parameters it is assumed that there are no losses to the surface of the solar cell, that the effect of the series resistance is negligible.

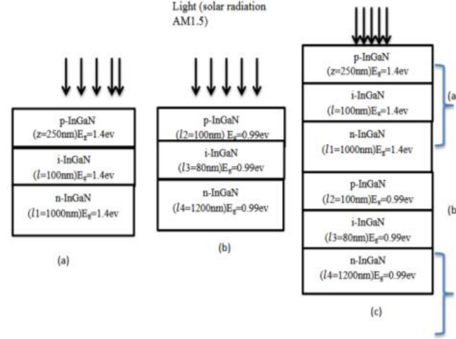

Fig. 1. (a) represents the top cell, (b) represents the bottom cell and (c) represents the tandem structure.

By modifying the theory of the proposed amorphous model of the silicon-based solar cell with PIN structure [4,5], the number of photons absorbed in a jth layer as a function of the energy is written as follows [4,5]:

$$f_j = \frac{A_j(E)\,F(E)}{E_j} \tag{1}$$

where F(E) represents the incident flow of solar radiation AM1.5 ($1000 w/cm^2$), E(=hυ) is the photon energy, $A_j(E)$ is the absorption j^{th} layer it gives as a follow [6]:

$$A_{absj} = \frac{I^j - I^{j+1}}{I_0} \tag{2}$$

I^j the light intensity which decreases exponentially with thickness, so before reaching the intrinsic layer [1]:

$$I(E,z) = I_0(E)e^{-\alpha(E)z} \tag{3}$$

I_0 the incident intensity of solar radiation AM1.5 ($1000 w/cm^2$), z the thickness of the layer P, and α(E) absorption coefficient as a function of energy is given by [7]:

$$\alpha(E) = \alpha_0\sqrt{\frac{E - E_g(x)}{E_g(x)}} \tag{4}$$

$E_g(x)$ is the gap energy of $In_xGa_{1-x}N$ and $\alpha_0 = 2 * 10^5 cm^{-1}$ (α_0 InGaN is supposed to be the same as GaN)[1]. $E_g(x)$ is the bandgap energy of InGaN as a function of x of the ternary alloy $In_xGa_{1-x}N$ which depends on temperature using the Vegard law, and can be expressed as follows [7]:

$$E_g(x,T) = (1-x){E_g}^{GaN}(\mathrm{T}) + x\,{E_g}^{InN}(\mathrm{T}) - b\,x\,(1-x) \quad (5)$$

where ${E_g}^{InN}$, ${E_g}^{GaN}$ are the forbidden energy bands of InN and GaN, respectively, x is the indium concentration in $In_xGa_{1-x}N$ and b=1.43 eV (the curvature parameter) [8].

The bandgaps of InN and GaN binaries as a function of temperature are expressed using Varshini's law [9,10]:

$${E_g}^{GaN}(\mathrm{T}) = {E_g}^{GaN}(T = 0^\circ K) - \frac{0.909\times10^{-3}\times T^2}{T+830} \quad (6)$$

$${E_g}^{InN}(\mathrm{T}) = {E_g}^{InN}(T = 0^\circ K) - \frac{0.245\times10^{-3}\times T^2}{T+624} \quad (7)$$

With ${E_g}^{GaN}(T = 0^\circ K)$=3.51 eV and ${E_g}^{InN}(T = 0^\circ K)$=0.72 eV [9,10].

The calculation of the absorption used in this simulation for the top cell given by equation (2) is expressed by [6]:

$$A_{pT} = [I_0 - I_0 \times \exp(-\propto_t \times z)]/ I_0 \quad (8)$$

$$A_{iT} = [I_0 \times \exp(-\propto_t \times z) - I_0 \times \exp(-\propto_t \times (z+l))]/ I_0 \quad (9)$$

$$A_{nT} = [I_0 \times \exp(-\propto_t \times (z+l)) - I_0 \times \exp(-\propto_t \times (z+l+l1))]/ I_0 \quad (10)$$

With $z, l, l1$ are thicknesses of each cell p, i, n for the top cell respectively.

The absorption in the bottom cell is defined by the product of the incident photons by the fraction of photons absorbed by the top cell, by the fraction of photons that penetrate in the bottom cell, we can express the absorption by:

$$A_{pB} = [I_0 \times (1 - \exp(-\propto_b \times (z+l+l1)) \times (1 - \exp(-\propto_b \times (l2)))]/ I_0 \quad (11)$$

$$A_{iB} = [I_0 \times \exp(-\propto_b \times (z+l+l1+l2) - I_0 \times \exp(-\propto_b \times (z+l+l1+l2+l3))]/ I_0 \quad (12)$$

$$A_{nB} = [I_0 \times \exp(-\propto_b \times (z+l+l1+l2+l3) - I_0 \times \exp(-\propto_b \times (z+l+l1+l2+l3+l4))]/ I_0 \quad (13)$$

With $l2, l3, l4$ are thicknesses of each layer p, i, n for the bottom cell respectively.

The short-circuit current density, J_{sc}, is obtained by the product of the number of load carriers by the collection efficiency [11]:

$$J_{SC} = q\chi \int \frac{A_j F(E)}{E_j}\, dE \quad (14)$$

where q electronic charge ($1.6*10^{-19}$ C)

And, χ is the collection efficiency of free carriers, defined by the ratio of the number of load carriers contributing to the photovoltaic current to the total number of photogenerated charge carriers. The efficiency of the collection is an important parameter to determine the performance of a solar cell. The collection efficiency in the intrinsic layer is obtained by [4,5].

$$\chi = \frac{\int_0^l (G-R)dx}{\int_0^l G dx} \cong \frac{G_0 l - \int_0^l R(x)dx}{G_0 l} \quad (15)$$

where G and R are the generation and recombination rate of load carriers respectively and l is the thickness of the intrinsic layer. The generation rate depends on the absorption of the intrinsic layer, which assumes constant $G_0 = G$ through the i layer.

The R(x) recombination rate is calculated by [11]:

$$R(x) = \frac{n(x)}{\tau_n} + \frac{p(x)}{\tau_p} \tag{16}$$

$\tau_n\ et\ \tau_p$ are the lifetime of the load carriers of the electrons and the holes respectively, $n(x)$ and $p(x)$ are the concentrations of electrons and holes respectively obtained by the resolutions of the equations of continuity and the transport in permanent regime [11]:

$$0{=}G_0 - \ R(x){+}\frac{1}{q}\frac{d}{dx}J_n(x) \tag{17}$$

$$0{=}G_0 - \ R(x){+}\frac{1}{q}\frac{d}{dx}J_p(x) \tag{18}$$

$$J_n(x) = q\mu_n n(x)E \tag{19}$$

$$J_p(x) = q\mu_p p(x)E \tag{20}$$

$J_n(x)$ and $J_p(x)$ are the current densities for the electron and holes respectively, E the electric field which is considered constant, μ_n, μ_p are the mobility of electrons and holes respectively. From the equation (17.16) and (19.20) we find [4.5]:

$$n(x) = \frac{G_0 l_p \tau_n}{l_p - l_n e^{-bl}}(1 - e^{-bx}) \tag{21}$$

$$p(x) = \frac{G_0 l_n \tau_p}{l_p - l_n e^{-bl}}(e^{-bx} - e^{-bl}) \tag{22}$$

With b=$l_n - l_p/-l_n l_p = -(2/l_c)$;

$$\int_0^l R(x)dx = \int_0^l (\frac{n(x)}{\tau_n} + \frac{p(x)}{\tau_p})dx = \frac{G_0 l_p l_n (e^{-bl}-1)}{l_p - l_n e^{-bl}} + lG_0 \tag{23}$$

From equation (15) find [4,5]:

$$\chi = \frac{1}{l}\frac{l_n l_p}{l_n exp\left(\frac{l}{l_c}\right) - l_p exp\left(-\frac{l}{l_c}\right)}\left[exp\left(\frac{l}{l_c}\right) - exp\left(-\frac{l}{l_c}\right)\right] \tag{24}$$

where $l_{n.p} = \sqrt{D_{n.p}\tau_{n.p}}$

D_n and D_p are the constants of diffusion of electrons and holes. They are defined by Einstein's relationship [12,13,14]:

$$D_n = \frac{K_B T}{q}\ \mu_n \tag{25}$$

$$D_p = \frac{K_B T}{q}\ \mu_p \tag{26}$$

With K_B Boltzmann's constant and T the temperature.

The model used is an analytical and empirical model proposed by Caughey and Thomas [15] in which temperature is taken into account.

$$\mu_{n,p} = \mu_{n,p1}\left(\frac{T}{300}\right)^{\alpha_{n,p}} + \frac{\mu_{n,p2}\left(\frac{T}{300}\right)^{\beta_{n,p}} - \mu_{n,p1}\left(\frac{T}{300}\right)^{\alpha_{n,p}}}{1+\left(\frac{N}{N_{n,p}^{crit}\left(\frac{T}{300}\right)^{\gamma_{n,p}}}\right)^{\delta_{n,p}}} \tag{27}$$

where N is the total concentration of doping, T temperature, the parameters used in the equation (26) are empirical to model the mobility of electrons and holes [16, 8, 17]. The parameters α, β, γ are taken equal to 1[18] when they are not experimentally available.

The lifetime model accredited in this modeling is activated by the parameter SRH is shown as followed [19, 20]:

$$\tau_{n,p} = \frac{\tau_{0(n,p)}}{1+N_{tolal}/N_{(n,p)}^{SRH}} \tag{28}$$

where $\tau_{0(n,p)} = 1.0 \times 10^{-7}(s)$ the lifetime of electrons and holes,

$N_{(n,p)}^{SRH} = 5.0 \times 10^{16}(cm^{-3})$ constants defining recombinant defect concentrations for electrons and holes.

N_{tolal} total concentration of defects and doping (cm^{-3})

The open circuit voltage, V_{coT} for the top cell and V_{coB} for the bottom cell is determined from the following expression [21]:

$$J = J_{sc} - J_{0T}\left(\exp\left(\frac{qv}{kT}\right) - 1\right) - J_{1T}(\exp\left(\frac{qv}{2kT}\right) - 1) \tag{29}$$

$$J = J_{SC} - J_{0B}\left(\exp\left(\frac{qv}{kT}\right) - 1\right) - J_{1B}\left(\exp\left(\frac{qv}{2kT}\right) - 1\right) \tag{30}$$

With J_{0T} is the saturation current of the upper cell

J_{1T} is the generation-recombination saturation current of the upper cell.

J_{0B} is the saturation current of the bottom cell.

J_{1B} is the generation-recombination saturation current of the bottom cell.

From the equation (14) the current density for each cell is determined.

$$J_{SCT} = J_{SCpT} + J_{SCiT} * \chi_T + J_{SCpT} \tag{31}$$

$$J_{SCB} = J_{SCpB} + J_{SCiB} * \chi_B + J_{SCpB} \tag{32}$$

J_{SC} we take into consideration that the minimum between the top cell and the bottom cell will be the current density.

The solution of equations (29) and (30) for J=0, to obtain the open-circuit voltage V_{coT} and V_{coB}, this solution is non-linear and must be solved numerically, the open-circuit voltage for the tandem structure is the sum of two voltages [22,23]:

$$V_{co} = V_{coT} + V_{coB} \tag{33}$$

With V_{coT}, V_{coB} open-circuit voltage for top and bottom cells respectively.

where $J_{0(T,B)}$ saturation current of the top and bottom cells respectively is given by :

$$J_{0(T,B)} = en_{i(T,B)}^2\left[\frac{1}{N_{a(T,B)}}\sqrt{\frac{D_{n(T,B)}}{\tau_{n(T,B)}}} + \frac{1}{N_{d(T,B)}}\sqrt{\frac{D_{p(T,B)}}{\tau_{p(T,B)}}}\right] \tag{34}$$

with $N_{a(T,B)}, N_{d(T,B)}$ are electron and hole concentrations of top and bottom cell respectively, , $N_{d(T,B)} = 2.5*10^{18}$; $N_{a\,(T,B)} = 5*10^{18}$ are the concentrations used in this study.

$J_{1(T,B)}$ Saturation current in the space load area is given by the relationship [24]:

$$J_{1(T,B)} = \frac{qn_i\, l_{(T,B)}}{2\tau_{(T,B)}} \tag{35}$$

where $n_{i(T,B)}$ the intrinsic load carrier concentration given by:

$$n^2_{i(T,B)} = N_{c(T,B)} N_{V(T,B)} \exp(\frac{-E_{g(T,B)}}{KT}) \tag{36}$$

where $N_c^{GaN} = 4.82 \times 10^{15} (\frac{m_\Gamma}{m_0})^{\frac{3}{2}} (T)^{\frac{3}{2}}$, $N_v^{GaN} = 8.9 \times 10^{15} (T)^{\frac{3}{2}}$

$N_c^{InN} = 4.82 \times 10^{15} \times (\frac{m_\Gamma}{m_0})^{\frac{3}{2}} (T)^{\frac{3}{2}}$, $N_v^{InN} = 10^{16} \times (T)^{\frac{3}{2}}$ [25].

From a linear interpolation (Vegard law) between the expressions of GaN and InN we find N_c and N_v of InGaN for the top and bottom cells.

We use in the modeling $m_0=9.109\times10^{-31}$ Kg the mass of the electrons at rest, $m_{eGaN}=0.2\ m_0$; $m_{hGaN}=0.8m_0$; $m_{eInN}= 0.11m_0$; $m_{hInN}=0.65\ m_0$ [26].

The maximum power is a point on the current-voltage curve I-V, which is expressed by the maximum output power P_{max}.

$$P_{max}=J_m V_m \tag{37}$$

where J_m,V_m correspond respectively to the values of I and V corresponding to the point P_{max}, FF the form factor calculated by [27]:

$$FF = \frac{P_{max}}{J_{sc}V_{co}} = \frac{J_m V_m}{J_{sc}V_{co}} \tag{38}$$

The conversion efficiency of a solar cell is given by [23]:

$$\eta = \frac{P_{max}}{P_{in}} = \frac{FF \times J_{sc} \times V_{co}}{P_{in}} \tag{39}$$

where P_{in} is the optical incident power of the solar radiation AM1.5 (1000w/cm^2) on the area of the solar cells.

3. Results and discussion

In this work, the theoretical simulation of a tandem solar cell with dual junctions PIN ($In_{0.62}Ga_{0.38}N$) PIN ($In_{0.81}Ga_{0.19}N$) that correspond to the twinning of energy bandgap as the top of the structure is 1.40 eV and the bottom of the structure is 0.99 eV at the temperature ranging from 300˚K to 450˚K, under illumination AM1.5.

Fig. 2 shows a strong absorption into the single bottom cell that increases with the increase of temperature; the cell is exposed to a part of the solar scepter to improve absorption, the deep penetration of photon in the infrared range improves the absorption of photons. The increase in the molar fraction in the solar cell decreases the energy of the forbidden band that allows the absorption of an only high-energy photon. The absorption in the cell top PIN ($In_{0.62}Ga_{0.38}N$) is less than the absorption in the cell bottom PIN ($In_{0.81}Ga_{0.19}N$) is due to the molar fraction that influences on bandgap energy. The increase in temperature leads to a slight increase in absorption in both cells.

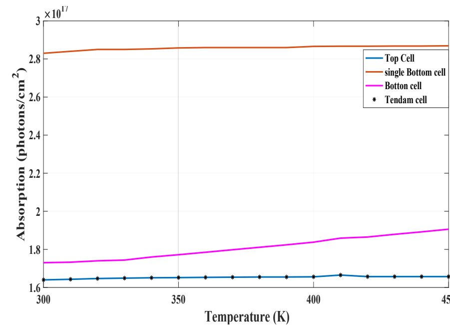

Fig. 2. Shows the absorption of the top and bottom cells, the single bottom cell, and the dual-junction (tandem) structure under illumination AM1.5 (1000 w/cm^2) calculated at temperatures ranging from 300˚K to 450˚K.

Fig. 3 shows that the current density of the bottom single cell is higher than the current density of the top cell due to the increase of the molar fraction, which decreases the bandgap energy that favors a strong absorption of the solar spectrum. The decrease of the bandgap gives a strong absorption of the photons that generate electron-hole pairs that will be collected, and the penetration of this quantity of photons to the bottom cell increases the current density as a function of the temperature. The current density of the single bottom cell is higher than that of the bottom cell, due to the reduction of the spectral light intensity illuminating the bottom cell. Since the current density of the dual junction (tandem) solar cell is the lowest current density produced by the two cells, which is similar to the top cell.

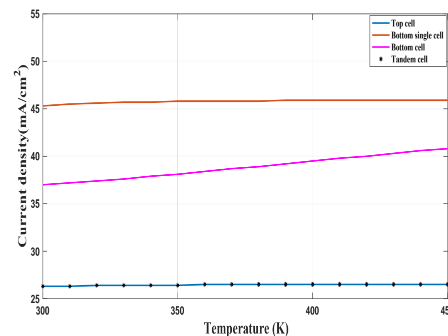

Fig. 3. The variation of the short-circuit current density of the both cells (top and bottom), the single bottom cell and the tandem structure as a function of temperature. The current density of each cell was calculated at temperatures ranging from 300˚K to 450˚K.

Fig. 4 shows that the open-circuit voltage of each solar cell was inversely proportional to the temperature, which means that the decrease of the open-circuit voltage with the increase of the temperature due to the decrease of the bandgap energy and the increase of the saturation current density of each cell. The open-circuit voltage of the top cell is higher than the open-circuit voltage of the single bottom cell and the bottom cell for each temperature due to their different energy of the bandgap of each solar cell; the higher the energy of the bandgap, the higher the open-circuit voltage. So, the open-circuit voltage of the dual-junction tandem cell and the sum of two voltages (top, bottom) cells is their decrease with the increase of temperature due to the decrease of the addition of two cells.

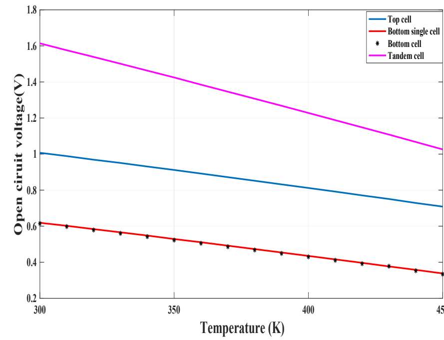

Fig. 4. Shows the open-circuit voltage of the top and bottom cell, single bottom cell, and the tandem cell PIN ($In_{0.62}Ga_{0.38}N$)/ PIN ($In_{0.81}Ga_{0.19}N$) as a function of temperature ranging from 300˚K to 450˚K.

Fig. 5 shows that the form factor of the solar cells decreases with increasing temperature; this decrease is due to the decrease of the open circuit voltage. It is noticeable that the form factor of the bottom cell and the single bottom cell is more affected by temperature than the top cell and tandem, which explains a reduction on the intensity.

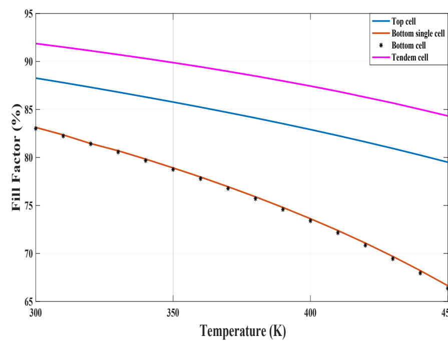

Fig. 5. Shows the variation of solar cell form factor as a function of the temperature ranging from 300˚K and 450˚K.

As the temperature increases, the conversion efficiency of the solar cells studied decreased. This decrease occurs due to a decrease in open-circuit voltage. Figure (6) shows that the efficiency of the bottom cell is lower than that of the single bottom cell due to the reduction in the irradiation of the solar spectrum, which means as the single bottom cell is illuminated by the whole solar spectrum. The effect of the thermalization and the temperature increase causes the excess energy of the high-energy carriers. For this reason, the thermalization effect is limited to the bottom cell because it is only illuminated by a part of the solar spectrum that low energy photons will be absorbed since the top cell has absorbed the high-energy photons. When the two cells PIN ($In_{0.62}Ga_{0.38}N$), PIN ($In_{0.81}Ga_{0.19}N$) are in series contact to have a dual-junction tandem cell, the decrease in efficiency with increasing temperature due to the decrease in the sum of the open-circuit voltage which decreases with increasing temperature.

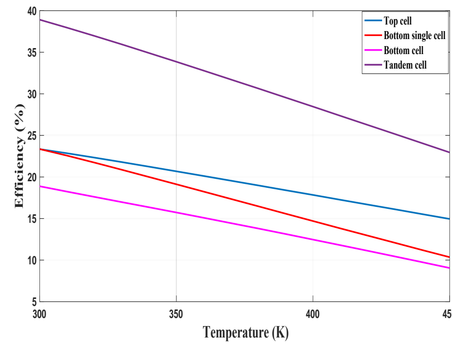

Fig. 6. Shows the variation an efficiency of the dual-junction (tandem) solar cell PIN ($In_{0.62}Ga_{0.38}N$)/PIN ($In_{0.81}Ga_{0.19}N$), the top and bottom cells, and the single bottom cell, with the temperature, was calculated for a temperature ranging from 300˚K to 450˚k.

4. Optimal structure

Based on the above results obtained using the ANOC calculation code, we can determine the current-voltage and voltage-power characteristics of solar cells with different molar fractions, the top cell PIN ($In_{0.62}Ga_{0.38}N$), the bottom cell PIN ($In_{0.81}Ga_{0.19}N$), single bottom cell, and tandem structure PIN ($In_{0.62}Ga_{0.38}N$)/PIN ($In_{0.81}Ga_{0.19}N$) with the optimal efficiency for the different structures are illustrated in figure (7) at 300˚K and under illumination AM1.5 (1000W/m^2), and the corresponding parameters are summarized in Table (1).

Table 1. The summary of the electrical parameters of the studied cells at 300˚K.

PV	Top cell	Bottom single cell	Bottom cell	Tandem cell
J_{sc}(mA/cm^2)	26.3	45.3	37.0	26.3
V_{co}(volt)	1.007	0.619	0.615	1.614
FF(%)	88.27	83.13	83.02	91.87
η(%)	23.35	23.36	18.88	38.92

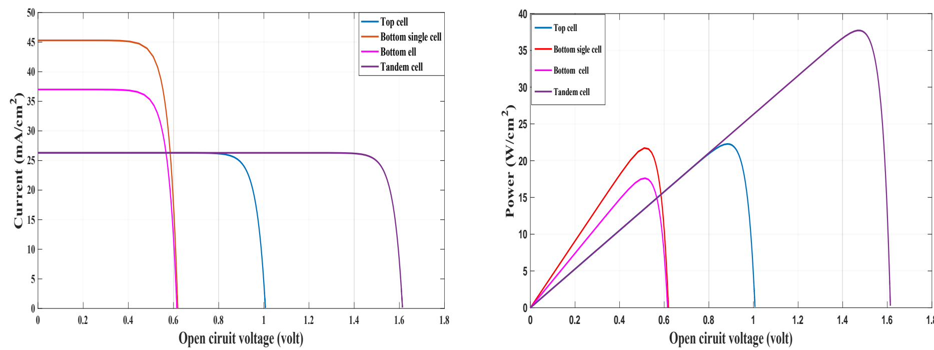

Fig. 7. The current-voltage and voltage-power characteristics of solar cells as a function of temperature at 300˚K.

5. Conclusions

In this study the influence of temperature on the following structures was simulated:
- An top PIN cell $In_{0.62}Ga_{0.38}N$,
- A bottom PIN cell $In_{0.81}Ga_{0.19}N$,
- A tandem structure $In_{0.62}Ga_{0.38}N$/ $In_{0.81}Ga_{0.19}N$.

Under AM 1.5 illumination varying the temperature from 300˚K to 450˚K.

The results obtained from the theoretical simulation show that the increase in temperature reduces the electrical parameters of the solar cell such as a decrease in the open-circuit voltage and efficiency of any cell and a decrease in the absorption and density of short circuit current.

This study allowed us to compare the performance of the PIN cells taken separately and the tandem structure while placing the large gap cell above and the small gap cell below, which allowed an increase in the total yield for the same area. Knowing that the temperature decreases the performance of each cell taken separately it is clear that the tandem structure compensates for this loss due to the increase in temperature. This is beneficial for small structures such as AM1.5 uses or even more so for use in AM0 outside the atmosphere or every inch must be exploited to the maximum, as in the case of space shuttles or promising solar cell aviation.

References

[1] E. Fred Schubert, Light Emitting Diodes (Cambridge University Press, New York), (2006).
[2] Junqiao Wu, Journal of Applied Physics **106**(1), 5 (2009).
[3] G. F. Brown, J. W. Ager, W. Walukiewicz, J. Wu, Solar Energy Materials and Solar Cells **94**(3), 478 (2010).
[4] P. Stulik, H. Singh, Non-Cryst. Solids **226**, 299 (1998).
[5] J. Hubin, A. V Shah, Philos. Mag. B **72**, 589 (1995).
[6] E. Mezzetti, A. Tagliaferro, E. Tresso, An Optimization Model for Amorphous Cells in Which Optical, Electrical and Recombination Properties are Specified (Dipatimento di Fisica Politecnico. Torino. Italia. April (1986)).
[7] I. Vurgaftman, J. R. Meyer, J. Appl. Phys**.** **94**, 3675 (2003).
[8] Muhammad Nawaz, Ashfaq Ahmad, Semiconductor Science and Technology **27**(3), 035019 (2012).
[9] V. Fiorentini, F. Bernardini, O. Ambacher. Appl. Phys Lett **80**, 1204 (2002).
[10] V. Gorge, A. M. Dubois, Z. Djebbour, K. Pantzas, S. Gautier, T. Moudakir, S. Suresh, A. Ougazzaden, Materials Science and Engineering B **178**, 142 (2013).
[11] Shih. W. Feng, Chih. Ming Lai, Chien. Hsun Chen, Wen. Ching Sun, Li. Wei Tu, J. Appl. Pys. **108**, 093118 (2010).
[12] Joachim Piprek, Semiconductor Optoelectronic Devices Introduction to Physics and Simulation, Academic Press, October (2013). Google-Books-ID : qqVuFz1kDp0C. 23, 46, 47, 48.
[13] Jiann S. Yuan, Juin Jei Liou, Semiconductor device physics and simulation. (Springer Science & Business Media, (2013). 46, 47, 48).
[14] Mijoe Joseph, Fundamentals of Semiconductor Physics, Anchor Academic Publishing (aap_verlag), May (2015). Google-Books-ID : aUg8CQAAQBAJ. 47
[15] D. M. Caughey, R. E. Thomas, Proceedings of the IEEE **55**(12), 2193 (1967).
[16] G. F. Brown, J. W. Ager, W. Walukiewicz, J. Wu, Solar Energy Materials and Solar Cells, **94**(3), 478 (2010).
[17] Shulong Wang, Hongxia Liu, Xin Song, Yulong Guo, Zhaonian Yang, Applied Physics A **114**(4), 1113 (2014)
[18] A. Adaine, Science des matériaux. Universite de Lorraine, (2018).
[19] M. Razeghi, Mohamed Henini, Optoelectronic Devices:III-nitrides, Gulf Profes- sional Publishing, (2004). Google-Books-ID : WnVljK6G7h4C. 51, 52.
[20] Analysis and Simulation of Semiconductor Devices. 51
[21] J. Nelson, the Physics of Solar Cell (Imperial College Press, (2003)), Ch. 6.

[22] X. Zhang, X. Wang, H. Xiao, C. Yang, J. Ran, C. Wang, Q. Hou, J. Li, Z. Wang, J. Phys. D Appl. Phys. **41**, 245104 (2008).
[23] Z. Li, H. Xiao. Wang, Q. Deng, L. Jing, L. Ding and X. Hou, Phys. B Condens. Matter **414**, 110 (2003).
[24] C. T. Sah, R. N. Noyce, W. Shockley, Proc. IRE **45**, 1228 (1957).
[25] E. Levinshtein, Michael L. Rumyantsev, Sergey S. Shur Michael, Properties of Advanced Semiconductor Materials GaN, AlN, InN, BN, SiC, SiGe.
[26] Vanessa Gorge, Caractérisation de materiaux et tests de composants des cellules solaire à base des nitrures des elements III-V. Autre [cond-mat.other]. Université Paris Sud-Paris XI, (2012). Francais. NNT : (2012)PA112076.
[27] B. Equer, Energie solaire photovoltaique (volume 1 : physique et technologie de la conversion photovoltaique), 1éré édition, ELLIPSE, Paris,(1993). (s.d).